Restoration of tumor suppressor protein with enhanced activity using engineered tRNAs to induce tumor regression

Bangyan Kong[1,2#], Zhetao Zheng[1,2#], Zeyuan Mi[1,2], Zhiyang Dou[1,2], Yuelin Yang[1], Yuxuan Shen[1], Liangzhen Dong[1,2], Jingru Lv[1,2], Ying Li[1,2], Qing Liang[1,2], Songlin Tian[2], Jiayu Wang[1,2], Hua Qiao[1,2], Qing Xia[1,2]✉

1. State Key Laboratory of Natural and Biomimetic Drugs, Peking University, Beijing, 100191, China.

2. Department of Molecular and Cellular Pharmacology, School of Pharmaceutical Sciences, Peking University, Beijing, 100191, China.

# These authors contributed equally to this work.

✉ Correspondence to: xqing@hsc.pku.edu.cn.

Abstract

Cancer develops through a gradual accumulation of mutations including nonsense mutations in tumor suppressor genes (TSGs), which drive tumor proliferation and progression due to the impairment or complete loss of tumor suppressor protein function[1-3]. The ability to restore functional tumor suppressor protein from mutant driver TSGs is a longstanding aspiration in cancer therapy, however, current strategies face formidable challenges in recovering proteins harboring heterogeneous mutations and circumventing dominant-negative effects exerted by endogenous mutant proteins. Therefore, the development of therapeutic interventions that are effective and generalizable across diverse nonsense mutations in cancer, to rescue endogenous mutant tumor suppressor proteins remains an urgent yet unmet need. Here we describe a “Double Suppressor Strategy” that engineered suppressor transfer RNA (sup-tRNA) could overcome nonsense mutations in key driver tumor suppressor genes, such as *TP53*, enabling the restoration of full-length p53 with its original or enhanced transcriptional activity through the precise incorporation of desired amino acids. Moreover, Optimized sup-tRNAs, designed guided by a computational model, could effectively suppress tumor cell proliferation by targeted readthrough of nonsense mutations in different tumor suppressor genes. In two xenograft models harboring nonsense mutant *TP53*, we observed up to a 60% reduction in tumor weight after sup-tRNA treatment, along with robust recovery of p53 expression and function, and no hematological or histological abnormalities detected. Our findings demonstrate the potential of sup-tRNA as a feasible and effective strategy to rescue and enhance tumor suppressor protein function, thereby preventing cancer development. As a novel therapeutic RNA, sup-tRNA provides a flexible strategy for targeting driver mutations in cancer, thereby expanding the potential of tRNA-based therapy in precision oncology.

Introduction

Cancer is a disease of uncontrolled proliferation by transformed cells harboring mutations in driver genes including tumor suppressor genes and oncogenes[1-3]. Notably, over half of the high frequency mutations occur in tumor suppressor genes[4,5], like *TP53*, mutations of which are found in approximately 42% of patients worldwide and their pivotal role in cancer development has been well established[6,7]. Our analysis of 315 driver tumor suppressor genes[2] revealed a striking correlation: genes with higher driver ability exhibit a significantly higher proportion of nonsense/truncating mutations ($p < 0.001$), whereas synonymous mutations show an inverse trend (Fig. 1a and Extended Data Fig. 1d)**.** This suggests that nonsense mutations, causing disastrous protein function loss, are evolutionarily selected in key tumor suppressors to promote tumor initiation (Fig. 1b and Extended Data Fig. 1). According to global cancer statistics reported by WHO, approximately 1 million new cancer cases annually harbor *TP53* nonsense mutations, leading to truncated inactive p53 proteins or complete loss of expression due to nonsense-mediated mRNA decay[8,9] (NMD). However, rescuing these mutations remains a significant challenge in current therapies[10]. Unlike targeting mutations in oncogenes by inhibiting or degrading aberrant oncoproteins directly, rescuing tumor suppressor gene mutations requires the restoration of functional tumor suppressor proteins, which poses a formidable challenge to bind and recover mutant proteins of heterogeneous inactivating mechanisms with a single agent[11-13]. Large-scale studies have identified potential drug molecules, such as Rezatapopt and arsenic trioxide (ATO), which could stabilize p53 mutants and restore their functional conformation, through inserting into the Y220C crevice[14] or filling the arsenic-binding pocket in p53 proteins, respectively[15-17]. However, their efficacy is clearly limited to p53 mutants with these specific binding sites and is not applicable for rescuing other *TP53* mutations, particularly nonsense mutations[11,18].

As nonsense mutations result in premature termination of p53 translation, a facile and promising strategy is to restore endogenous full-length p53 by translational readthrough of nonsense codons during protein synthesis, avoiding undesirable adverse effects associated with exogenous p53 overexpression and the dominant-negative effects of truncated mutant proteins often observed in conventional gene therapy. In this context, developing therapeutic agents capable of recognizing and overriding only three nonsense codons (UAG, UAA, UGA) could address diverse *TP53* nonsense mutants, sparking renewed enthusiasm in recent years. To date, myriad lead compounds, including aminoglycoside antibiotics and nucleoside analogs, have shown potential in overcoming cancer-derived *TP53* nonsense mutations and inhibiting tumor growth[19-22]. However, the reported readthrough approaches have yet to meet clinical needs, primarily due to their low efficiency (<10%) in most cases and the non-specific insertion of random amino acids in response to nonsense mutations, which may lead to the restoration of deleterious missense p53 mutants[23]. Suppressor tRNA (sup-tRNA), derived from natural transfer RNAs, could recognize and pair with the nonsense codon during translation elongation, and enables the incorporation of a specific amino acid at the targeted nonsense mutation, thus restoring the production and function of the full-length protein[24-26]. Given the high efficiency, low toxicity, and minimal safety concerns associated with sup-tRNA in treating inherited diseases caused by nonsense mutations, we anticipate that it also holds great promise for addressing nonsense mutations in human cancer.

In this work, we employ sup-tRNAs designed guided by nonsense mutation type in TSGs and a computational model, to incorporate specific amino acids through nonsense readthrough with an efficiency of up to 70%, restoring the

expression of functional p53 proteins that trigger apoptosis in *TP53* nonsense mutant human cancer cells. Compatible with current delivery systems, sup-tRNA has also exhibited strong anti-tumor efficacy in mouse models without observable abnormalities, underscoring the feasibility and robustness of tRNA-based nonsense readthrough strategy in cancer therapy.

Results

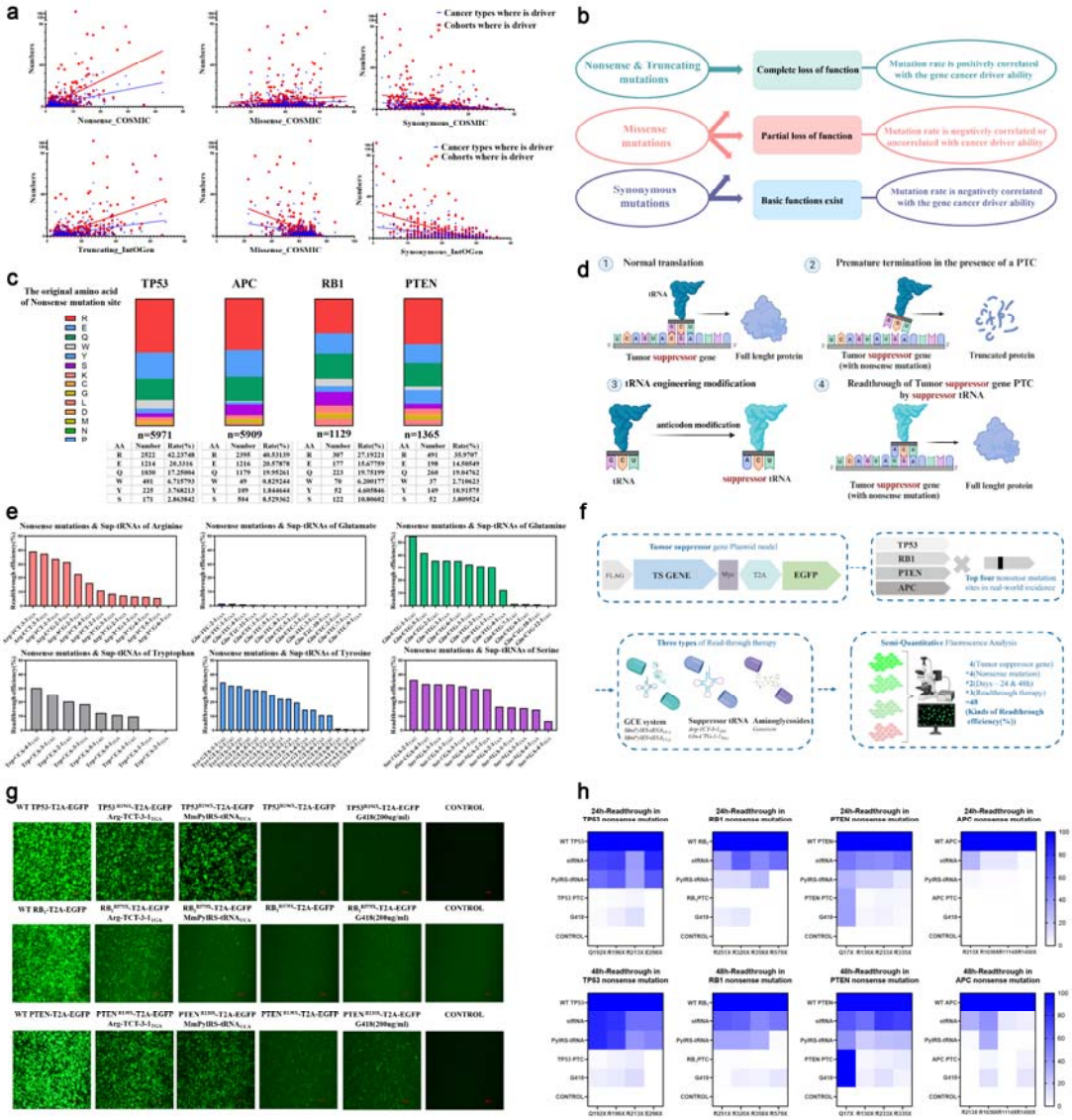

Fig.1 | The efficacy of sup-tRNA in overcoming nonsense mutations within tumor suppressor genes. a, Scatter plots of the proportion of mutation types (nonsense/ truncating mutation, missense

mutation, synonymous mutation) and the number of driver cancer types and cohorts in the Catalogue of Somatic Mutations in Cancer (COSMIC) and Integrative OncoGenomics (IntOGen) for mutational cancer driver tumor suppressor genes. **b**, The hypothesis explaining the correlation between the proportion of driver tumor suppressor genes mutation types and driver ability. Based on the existing theories, nonsense mutation most leads to the complete loss of function thus missense mutation may cause complete loss of function or partial loss of function. The synonymous mutation leads to a partial loss of function or basic function. The variability in different mutation fates can rationally explain the correlation described above. **c**, Classification of nonsense mutations according to their original codons and corresponding amino acids, and statistics of the mutation rates in tumor suppressor genes including *TP53*, *APC*, *RB1*, and *PTEN*, based on data adapted from COSMIC. **d**, Schematics of engineering natural transfer RNA (tRNA) to suppressor tRNA (sup-tRNA) for nonsense mutations readthrough in tumor suppressor transcripts. **e**, Quantification of readthrough efficiency of sup-tRNA encoding highly mutated amino acid defined in (**c**) using the dual-luciferase reporter assay. **f**, Construction of surrogate reporters containing nonsense mutant tumor suppressor genes and EGFP genes and the assay to compare the efficacy of sup-tRNA, GCE system, and G418 to overcome nonsense mutations in reporters, by measuring the downstream fluorescence expression. **g-h**, Microscopy images (**g**) and quantification (**h**) of GFP positive cells showing differential readthrough efficiencies of above three approaches. Consistent results were obtained independently for at least three biological replicates (in e). All data shown from HEK 293T cell experiments are mean of three biological replicates. (in **g**, **h**). Scale bar=100 μm.

Engineering sup-tRNAs to target nonsense mutations in *TP53*

We first analyzed the types of amino acids affected by nonsense mutations in the four vital tumor suppressor genes TP53, APC, RB1, and PTEN. The amino acids involved in these mutations were similar across these genes, primarily consisting of arginine (Arg), glutamic acid (Glu), and glutamine (Gln) (Fig. 1c). With the exception of glutamic acid, all frequently mutated amino acids had corresponding suppressor tRNAs capable of inducing nonsense readthrough by up to 55%, offering potential for the restoration of tumor suppressor proteins (Fig. 1d, e). Next, we constructed a series of surrogate reporters harboring nonsense mutant tumor suppressor genes and EGFP genes linked by a 2A peptide sequence, and employed sup-tRNAs to induce targeted readthrough of nonsense codons (UAG, UGA) to permit the downstream enhanced green fluorescent protein (EGFP) expression, allowing us to measure the readthrough efficiency through monitoring EGFP level (Fig. 1f). Though readthrough efficiency varies among different genes, we found that sup-tRNA

consistently outperforms the documented readthrough-promoting agent G418 (geneticin), achieving up to a 12.8-folds increase in efficiency (Fig. 1g, h). These results indicate that sup-tRNA can efficiently overcome nonsense mutations in tumor suppressor genes, inducing nearly 70% readthrough in nonsense mutant *TP53*.

To further investigate the capability of sup-tRNAs for the functional restoration of p53, we co-transfected NCI-H1299 cells (*TP53*-null) with sup-tRNAs, the p53 reporter, and a genetically encoded sensor, which allowed us to characterize full-length p53 protein expression via green fluorescence and assess its transcriptional activity restoration through red fluorescence (Fig. 2a and Extended Data Fig. 2). We found that sup-tRNAs carrying glutamine or arginine were able to rescue the expression and function of the frequent p53 mutants Q192X and R196X, albeit with varying efficiencies (Fig. 2b, c and Extended Data Fig. 2b, c). Furthermore, functional restoration exhibited a significant correlation with readthrough efficiency (Fig. 2b, c and Extended Data Fig. 2b, c). However, when applying the high-efficiency sup-tRNAs to address other COSMIC-reported p53 mutants harboring UAG or UGA nonsense mutations, we observed that the function of two mutants (G266X and Y234X) was not restored, despite the recovery of full-length protein expression (Fig. 2b and Extended Data Fig. 2b). By analyzing Y234X and G266X variants based on p53 crystal structure, we speculated that mischarging of Y234Q and G266R in p53, induced by sup-tRNA^{Gln} and sup-tRNA^{Arg}, may be deleterious (Fig. 2e). This is primarily attributed to the disruption of a hydrophobic core around Y234 and the formation of new hydrogen bonds between G266 and adjacent residues, potentially compromising the p53-DNA binding interface (Fig. 2e). Therefore, a reliable approach for restoring p53 activity necessitates the simultaneous consideration of readthrough efficiency and the functional impact of the incorporated amino acid.

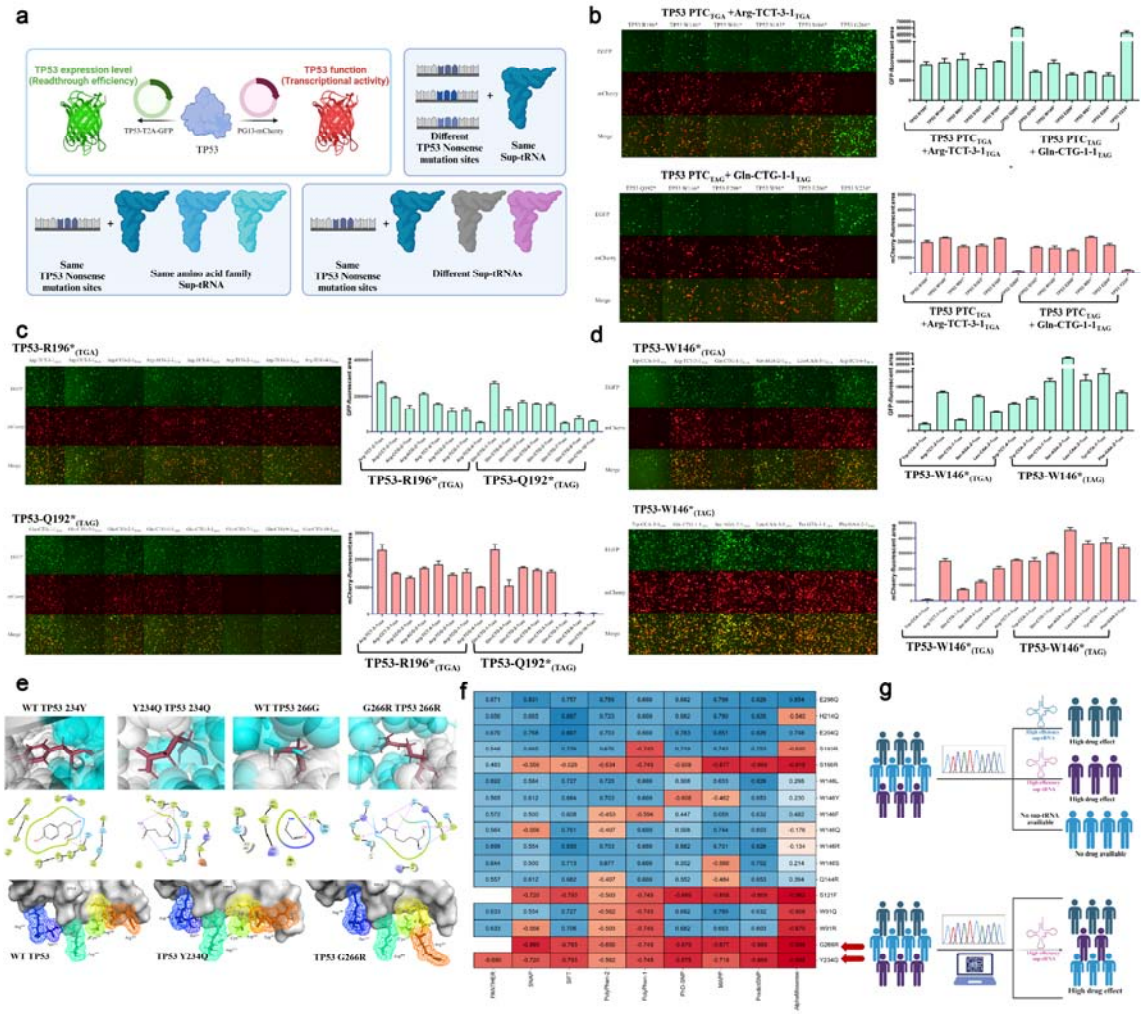

Fig.2 | Characterization of sup-tRNA in recovering p53 expression and function. a, Schematic of a genetically encoded reporter system to measure the expression and function of p53 via dual-fluorescence detection, which is designed for sup-tRNA efficiency characterization. **b**, Representative microscopy images (left) and quantification of GFP and mCherry positive cells (right) show p53 expression and function in NCI-H1299 cells with 12 kinds of nonsense mutations after sup-tRNA Arg-TCT-3-1$_{TGA}$ and Gln-CTG-1-1$_{TAG}$ readthrough. Data are mean ± s.d. of three biological replicates. Scale bars = 100 μm. **c**, Representative microscopy images (left) and quantification of GFP and mCherry positive cells (right) show p53 expression and function in NCI-H1299 cells with *TP53* R196*& *TP53* Q192* nonsense mutations after 8 kinds of arginine (R) and 8 kinds of glutamine (Q) sup-tRNAs readthrough. Data are mean ± s.d. of three biological replicates. Scale bars = 100 μm. **d**, Representative microscopy images (left) and quantification of GFP and mCherry positive cells (right) show p53 expression and function in NCI-H1299 cells with *TP53* W146* nonsense mutations after 7 amino acids while 12 kinds of high-efficiency sup-tRNAs readthrough. Data are mean of three biological replicates. Scale bars = 100 μm. **e**, Verified deleterious p53 variants mutant site amino acid residues and intermolecular forces. The first and third panels show the 234Y, and 266G structures of wild-type (WT) p53 DBD (2AC0), respectively. The other panels are drawn by mutating 234Y, 266G residue in wild-type DBD (2AC0) into the indicated residues in PyMOL and Schröder. The panels below show the close-up

view of the wild-type and verified deleterious p53 DNA binding peptides and DNA. The side chains of the six classic DNA binding residues are shown as sticks. **f**, Predictive and functional profile of p53 previous variants. The heat map corresponds to the predictive impact of each p53 variant ranging from -1 (red) to 1 (blue), with the lowest score being the most deleterious. Scores from the 9 algorithms in the panels including AlphaMissense, MAPP, PANTHER, PhD-SNP, PolyPhen-1, PolyPhen-2, SIFT, and SNAP. Red arrows indicate previous verified deleterious p53 variants. **g**, With the help of analysis by computational tools, restoration of nonsense mutations to neutral mutations by sup-tRNAs with high readthrough efficiency would be a good choice.

Computationally optimized screening of sup-tRNAs for enhanced p53 activity restoration

To this end, we developed a computational tool[27,28] to predict the functional impact of incorporated amino acids, facilitating the selection of optimal sup-tRNAs (Fig. 2f and Extended Data Fig. 4e). Using the p53-E204X mutant cancer cell line containing a UAG codon, we assessed its expression and functional restoration following readthrough induced by sup-tRNAs carrying different amino acids (Extended Data Fig. 4a). Consistent with the prediction, we found that sup-tRNA^{Phe}, sup-tRNA^{Tyr}, and sup-tRNA^{Trp} failed to restore p53 transactivation function due to the insertion of undesired amino acids, despite achieving high readthrough efficiencies (Extended Data Fig. 4b, c). Moreover, even when the original amino acid could not be restored due to the low readthrough efficiency of the corresponding sup-tRNA^{Glu}, high-efficiency sup-tRNAs, such as sup-tRNA^{Gln} and sup-tRNA^{Ser}, served as effective alternatives to rescue p53 function, provided that the incorporated amino acid, as predicted, does not disrupt the protein structure (Extended Data Fig. 4g). Further investigation also confirmed the robustness of this alternative strategy in restoring other functional p53 mutants (Extended Data Fig. 4), however, we noticed that some recovered p53 variants showed superior transcriptional activity compared to wild-type p53 proteins, for instance, sup-tRNA^{Gln} outperformed sup-tRNA^{Trp} in functional restoration of p53-W146X mutant (Fig. 2d and Extended Data Fig. 2d), even though the latter enabled recovery of wild-type p53 proteins.

These observations can be mechanistically explained by two critical determinants governing p53 functional restoration. First, when the incorporated amino acid induces minimal structural perturbation to native conformation of p53, sup-tRNAs with higher readthrough efficiency, such as sup-tRNA^{Gln}, sup-tRNA^{Arg}, and sup-tRNA^{Ser}, can achieve superior functional restoration (Fig. 2 and Extended Data Fig. 2). Second, in cases where readthrough efficiencies are comparable across different sup-tRNAs, the identity of the restored amino acid becomes particularly crucial. Notably, specific amino acid substitutions such as S121F, Q144R, and H214Q, resulted in p53 variants displaying enhanced anti-cancer function compared to wild-type p53 (Fig. 4e,f and Extended Data Fig. 5), which is consistent with previous reports[29]. Therefore, by leveraging the capacity of tRNAs to precisely incorporate desired amino acids during protein translation, we could restore p53 variants with retained or even enhanced functions, supported by computational guided sup-tRNA selection (Fig. 2f, g and Extended Data Fig. 4e, i). We also noted that a recent investigation employed CRISPR-mediated homology-directed repair to engineer 9,225 p53 variants in cancer cells, covering over 94% of cancer-associated missense mutations, and mapped their effects on p53 function[30]. These precious data are also helpful for choosing specific sup-tRNA for certain TP53 nonsense mutations.

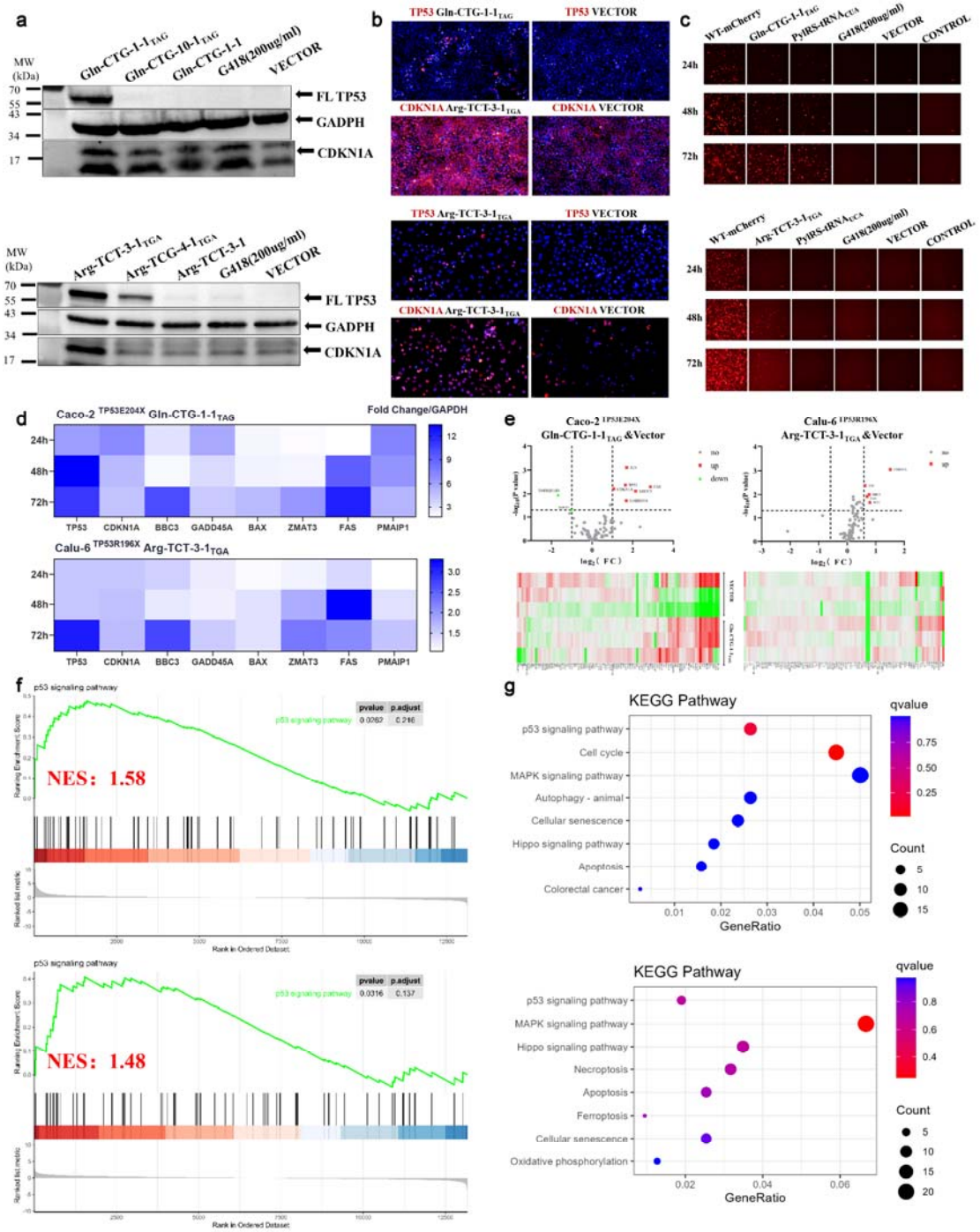

Fig.3 | Sup-tRNA rescues endogenous full-length p53 expression and restores its transcriptional activity. a, Western blot analysis of full-length p53 recovery and protein expression from its target gene *CDKN1A* in Calu-6 & Caco-2 cells treated with sup-tRNA, corresponding tRNA, vector, and G418 for 48 hours, respectively. **b**, Representative microscopy images of immunofluorescence for full-length p53 and CDKN1A in Calu-6 & Ccao-2 treated with sup-tRNA or vector for 48h. Scale bars= 20∟μm. Data shown here were representative examples from n=3 independent biological replicates. **c**, Representative microscopy images showing the transcriptional activity of endogenous p53 in Calu-6 & Caco-2 cells. Data

shown here were representative examples from n=3 independent biological replicates. **d**, Quantification of mRNA levels of *TP53* and its target genes *CDKN1A*, *BBC3*, *GADD45A*, *BAX*, *ZMAT3*, *FAS*, and *PMAIP1* after sup-tRNA treatment in Calu-6 cells and Caco-2 cells for 48h by qRT-PCR. All the mRNA expression levels are normalized to *GAPDH*. Data are represented as mean for n=3 independent biological replicates. **e**, Significant differential expressed of p53-relatived transcripts are determined by p53 PCR array on Calu-6 & Caco-2 treated with sup-tRNA, or vector control, n=3. **f-g**, Gene Set Enrichment Analysis (**f**) and KEGG pathway enrichment analysis (**g**)of p53 signaling pathways on Calu-6 & Caco-2 treated with sup-tRNA, or vector control, n=3.

Harnessing sup-tRNAs to overcome endogenous *TP53* nonsense mutations

Genomic analyses from COSMIC and intOGen databases have consistently identified *TP53* nonsense mutations as one of the most prevalent genetic alterations in non-small cell lung carcinoma (NSCLC) and colorectal cancer (CRC) (Extended Data Fig. 3a, b). TCGA data further highlight TP53 as the most critical driver gene in both NSCLC and CRC (Extended Data Fig. 3c). Therefore, we further investigated the efficacy of sup-tRNAs using NSCLC cell line Calu-6 (p53-R196X) and CRC cell line Caco-2 (p53-E204X), whose nonsense mutant *TP53* genes have been verified by whole-genome sequencing (Extended Data Fig. 3d). In Calu-6 cells, sup-tRNA$^{\text{Arg-TCT-3-1}}{}_{\text{TGA}}$, engineered from an arginine-carrying tRNA with a UCU anticodon, effectively restored high levels of full-length p53 expression (Fig. 3a). In contrast, G418 treatment resulted in only minimal p53 recovery, comparable to the tRNA$^{\text{Arg-TCT-3-1}}$ control and even significantly lower than that achieved with the low-efficiency (~6%) sup-tRNA$^{\text{Arg-TCG-4-1}}{}_{\text{TGA}}$ (Fig. 3a). In Caco-2 cells, sup-tRNA$^{\text{Gln-CTG-1-1}}{}_{\text{TAG}}$ also yielded a robust restoration of full-length p53 protein expression compared to other groups, as determined by western blot analysis (Fig. 3a). The recovery of p53 transactivation function was confirmed by red fluorescent encoded by the sensor (Fig. 3c) and increased expression of cyclin-dependent kinase inhibitor 1A (CDKN1A), a major downstream target of p53 activity, and further validated through immunostaining (Fig. 3b).

Classically, p53 functions mainly as a sequence-specific transcription factor

that can bind to p53 response element and activate the transcription of target genes. To evaluate the transcriptional activity of restored p53, we examined the expression levels of its target genes using RT-qPCR. Our results showed that the RNA expression levels of p53 and its downstream targets were upregulated to varying degrees in both Calu-6 and Caco-2 cell lines (Fig. 3d). Notably, the extent of upregulation increased over time, suggesting that sup-tRNA may prevent *TP53* mRNA with nonsense mutations from degradation by nonsense-mediated mRNA decay[9] (NMD), thereby promoting full-length p53 production for transactivation. To further confirm the efficacy of sup-tRNA in reactivating p53-related genes, we performed a PCR array analysis. In Calu-6 cells, RNA expression levels of p53 target genes, including *CDKN1A* and *BBC3*, were differentially upregulated following readthrough restoration of p53 (Fig. 3e). Similarly, in Caco-2 cells, RNA expression levels of *TP53* and its downstream targets were differentially upregulated, with the most pronounced increase observed in *FAS*, consistent with RT-qPCR results (Fig. 3e).

Moreover, RNA-seq analysis enabled us to assess the global influence of sup-tRNA on the transcriptomes of Caco-2 and Calu-6 cells. Gene Set Enrichment Analysis (GSEA) revealed that, compared with the control group, sup-tRNA treatment significantly upregulated the p53 signaling pathway in tumor cells from both Caco-2 (NES = 1.58, $p = 0.0262$) and Calu-6 (NES = 1.48, $p = 0.0316$) (Fig. 3f). KEGG analysis further highlighted enrichment in the p53 signaling pathway, MAPK signaling pathway, and cell cycle (Fig. 3g). Specifically, sup-tRNA treatment led to upregulation of the p53 signaling and apoptosis pathways, while downregulating the MAPK signaling, cell cycle, and Ras signaling pathways (Fig. 3g).

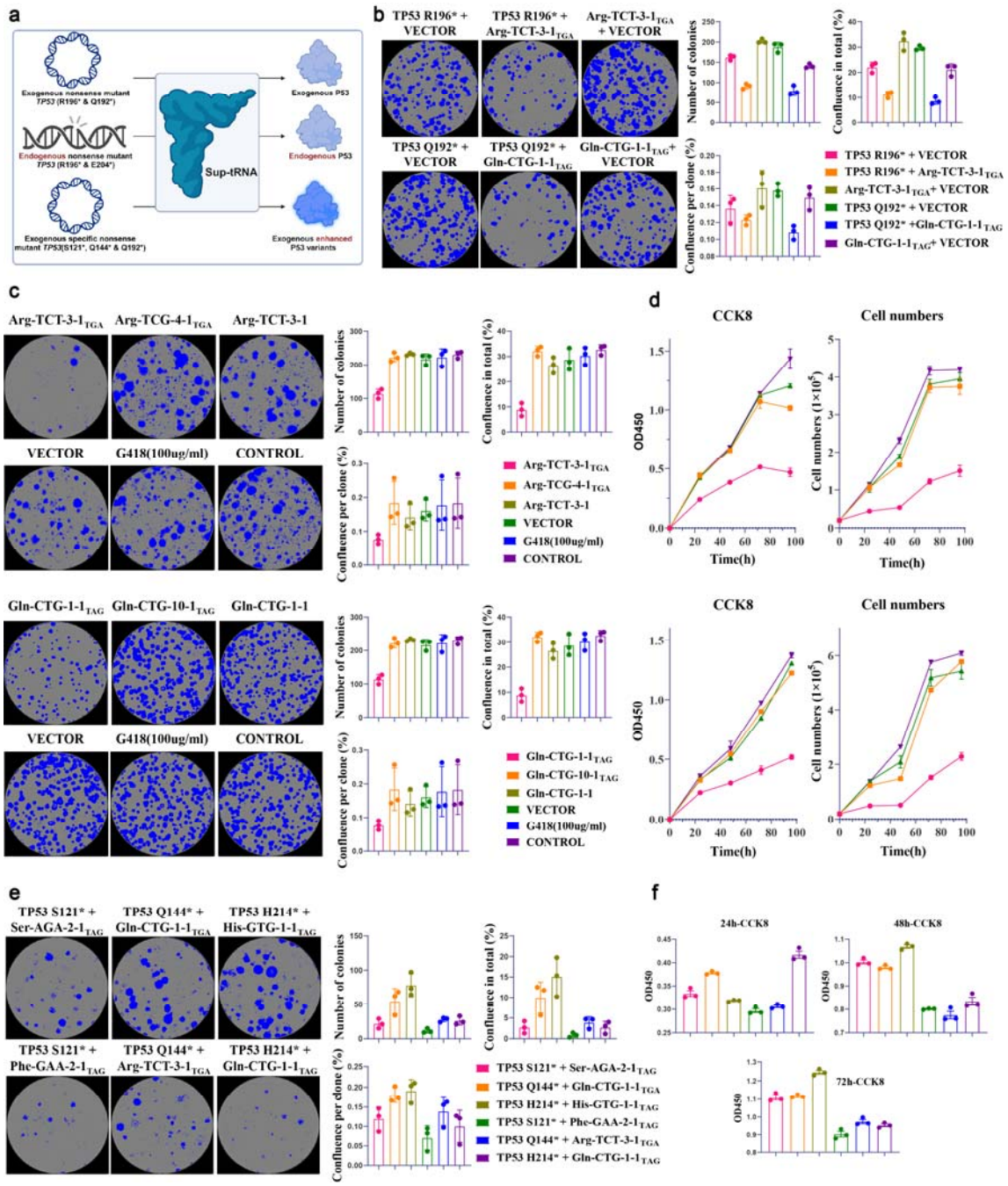

Fig.4 | Sup-tRNA elicits antiproliferation activity through p53 restoration. a, Schematic workflow for measure antiproliferative effects mediated by p53 restoration via sup-tRNA readthrough. **b**, Sup-tRNA in the presence of *TP53* exogenous nonsense mutation reduces the colony formation in human NCI-H1299 cells. Colonies are stained with crystal violet staining solution and counted after 10-12∟days of culture. Colony images are acquired by Incucyte SX5 and processed and analyzed by Incucyte 2022B Rev2. Data are represented as mean∟±∟SEM, n∟=∟3. **c**, Sup-tRNA treatment reduce the colony formation in human Calu-6 (above) & Caco-2 (below) cell which have genomic *TP53* nonsense mutation. Colonies are stained with crystal violet staining solution and counted after 10-12∟days of culture. Colony images are acquired by Incucyte SX5 and processed and analyzed by Incucyte 2022B Rev2. Data are

represented as mean∟±∟SEM, n∟=∟3. **d** Cell proliferation curve was measured by CCK-8 (left) and cell count assay (right). After transfecting human Calu-6 (above) & Caco-2 (below) cell for 8 hours, the cells are digested, spread in plates and further measured. Data are represented as mean∟±∟SEM, n∟=∟3. **e**, The sup-tRNA "break-bad" strategy compared to the strategy restore as wild-type p53 reduces the colony formation in human NCI-H1299 cell which introduce exogenous *TP53* nonsense mutation. Colony images are acquired by Incucyte SX5 and processed and analyzed by Incucyte 2022B Rev2. Data are represented as mean∟±∟SEM. N∟=∟3. **f**, CCK8 shows the sup-tRNA "break-bad" strategy compared to the strategy restore as wild-type p53 had a stronger growth inhibitory effect on the human NCI-H1299 cell which introduces exogenous *TP53* nonsense mutation.

Suppressing tumor cell proliferation by restoring p53 function

To verify that sup-tRNA could inhibit tumor cell growth by suppressing nonsense mutations in the *TP53* gene, we transfected *TP53*-null NCI-H1299 cells with both a nonsense mutant *TP53* and sup-tRNA, or with either component individually (Fig. 4a). The colony formation assay demonstrated that sup-tRNA exerted tumor-suppressive effects only in the presence of *TP53* nonsense mutations readthrough, leading to approximately a 60% reduction in colony number, a 70% decrease in total colony area, and a 30% reduction in the average area of individual clones (Fig. 4b). In contrast, sup-tRNA alone did not exhibit significant proliferation-inhibitory effects in tumor cell lines lacking nonsense mutant *TP53* (Fig. 4b).

Next, we sought to evaluate the efficacy of sup-tRNA in suppressing the proliferation of tumor cells harboring endogenous *TP53* nonsense mutations (Fig. 4a). Treatment with high-efficiency sup-tRNAs resulted in significant inhibition of cell growth and reduced cell viability. In Calu-6 cells, restoration of p53 using sup-tRNA$^{\text{Arg-TCT-3-1}}{}_{\text{TGA}}$ resulted in a notable reduction in colony number, total colony area, and individual clone size, outperforming both G418 treatment and the low-efficiency control, consistent with previous findings (Fig. 4c, d). Similar results were also observed in Caco-2 cells, further highlighting the robustness of sup-tRNA across different cell lines (Fig. 4c, d). Given that nonsense mutant *TP53* could produce missense p53 variants with enhanced transactivation function[29] via sup-tRNA-mediated readthrough (Fig. 4a), we

further demonstrated the augmented efficacy of restored p53 variants S121F, Q144R, H214Q in inhibiting tumor cell growth (Fig. 4e, f). As conventional gene therapy could only introduce wild-type p53 that may be neutralized by endogenous truncated p53 in a dominant-negative effect[31], high-efficiency sup-tRNAs could directly convert truncated p53 into functional or even enhanced p53 variants[29] in suppressing tumor cell proliferation, providing a plausible strategy, termed as "break-bad", to further improve the efficacy of translational readthrough in tumor inhibition(Fig. 4e, f and Extended Data Fig. 5).

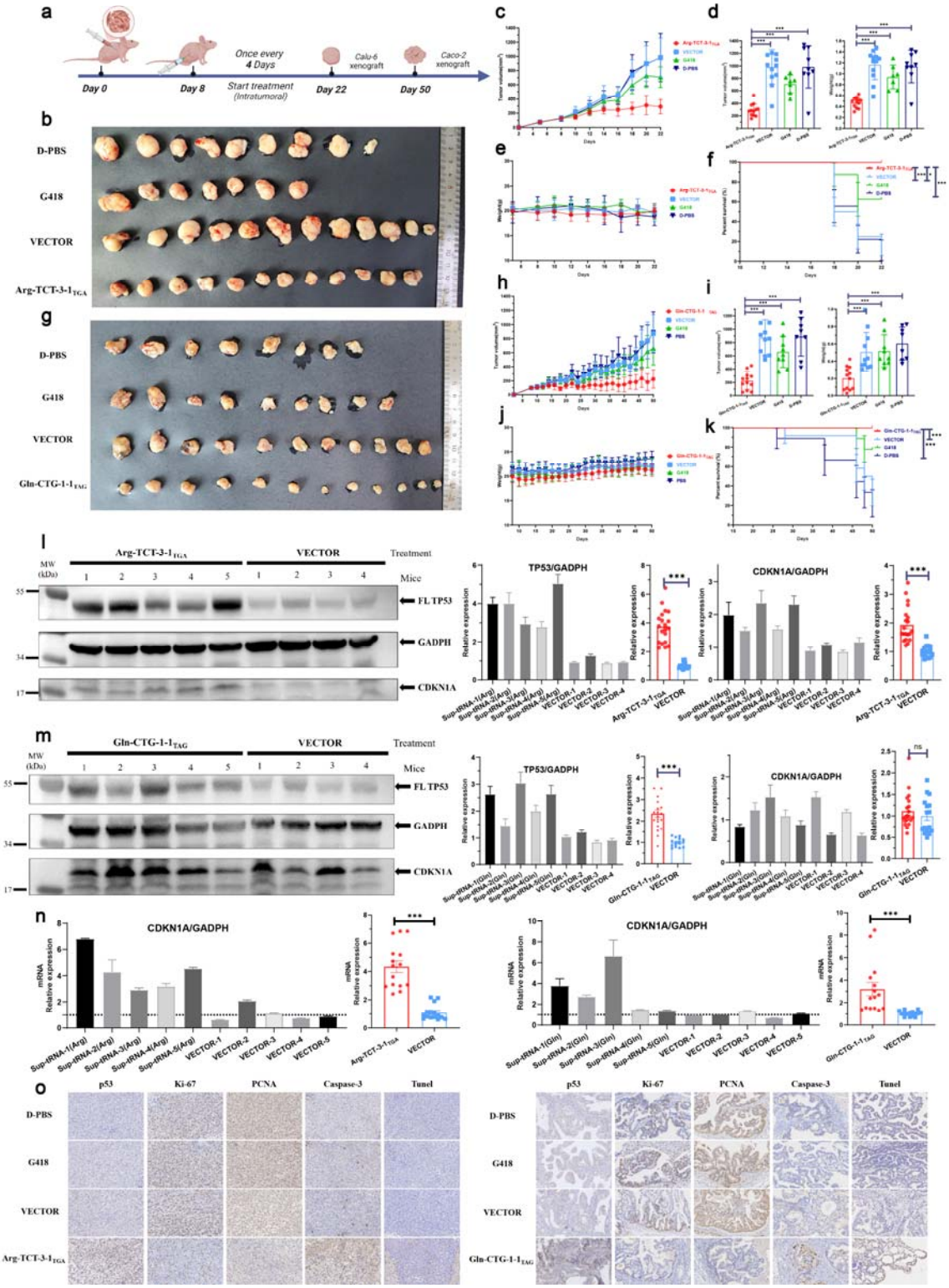

Fig.5 | Therapeutic efficacy of sup-tRNA therapy *in vivo.* **a**, Schematic of therapeutic evaluation of sup-tRNA therapy. **b**, Images of Calu-6 xenograft excised tumors. **c-f**, Tumor growth curves (**c**), volumes

and weights of tumor collected on Day 22 (**d**), weight curve (**e)**, and Kaplan-Meier survival curves (**f**) in Calu-6 xenograft model after sup-tRNA Arg-TCT-3-1_{TGA} therapy. *P*-values were calculated by one-sided t test. **g**, Images of Caco-2 xenograft excised tumors. **h-k**, Tumor growth curves (***h***), volumes and weights of tumor collected on Day 50 (**i**), weight curve (**j**), and Kaplan-Meier survival curves (**k**) in Caco-2 xenograft model after sup-tRNA Gln-CTG-1-1_{TAG} therapy. *P*-values were calculated by one-sided t test. **l**, Western blot analysis of full-length p53 recovery and protein expression from its target gene *CDKN1A* in Calu-6 xenograft treated with sup-tRNA (left) and quantification of the expression of each indicated protein relative to GAPDH expression, and normalized to the control mean (right). *P*-values were calculated by one-sided t test. **m**, Western blot analysis of full-length p53 recovery and protein expression from its target gene *CDKN1A* in Caco-2 xenograft treated with sup-tRNA (left) and quantification of the expression of each indicated protein relative to GAPDH expression, and normalized to the control mean (right). *P*-values were calculated by one-sided t test. **n**, Quantification of mRNA levels of p53 target genes *CDKN1A* in Calu-6 (left) and Caco-2 (right) xenograft by RT-PCR. All the mRNA expression levels are normalized to *GAPDH*. Data are represented as mean ± SEM and individual data points shown for n = 3 independent biological replicates. *P*-values were calculated by one-sided t test. **o**, Immunohistochemistry analysis of Calu-6 (left) and Caco-2 (right) xenograft including p53, proliferation and apoptosis markers after corresponding treatments. Scale bar=50 μm. Data shown here were representative examples from n=3 independent biological replicates.

In vivo **efficacy of sup-tRNA in *TP53* nonsense mutant xenograft**

We next utilized cell-line-derived xenograft (CDX) mouse models to investigate whether sup-tRNA could restore p53 protein expression from *TP53* nonsense mutations *in vivo* and inhibit tumor growth. Six-week-old immunodeficient nude mice were implanted with either Calu-6 or Caco-2 cells to generate xenograft models harboring *TP53* nonsense mutations, and were treated with sup-tRNA via intra-tumoral delivery once the tumor volume reached approximately 200 mm^3 (Fig. 5a). For the NSCLC Calu-6 xenograft model with p53-R196X, we treated the mice with sup-$tRNA^{Arg\text{-}TCT\text{-}3\text{-}1}{}_{TGA}$ and G418 as a positive control. The tumor growth curve of the sup-$tRNA^{Arg\text{-}TCT\text{-}3\text{-}1}{}_{TGA}$ group showed a significantly slower growth rate compared to the control groups after the first treatment (Day 8), resulting in a tumor volume reduction of approximately 70% and no mortality by the study endpoint (Day 22) (Fig. 5b-f). In terms of functional p53 recovery, sup-tRNA treatment resulted in a 3.7-fold increase in full-length p53 expression and a 1.9-fold increase in downstream CDKN1A expression compared to vector treatment (Fig. 5l). RT-qPCR analysis also revealed a 4.3-fold upregulation of *CDKN1A* transcripts in the sup-tRNA group

relative to vector (Fig. 5n). Consistently, sup-tRNA$^{Gln\text{-}CTG\text{-}1\text{-}1}{}_{TAG}$ treatment also significantly attenuated tumor progression in the CRC Caco-2 xenograft harboring p53-E204X, with no treatment-related mortality observed by the endpoint (Day 50) (Fig. 5g-k). Moreover, both protein levels of p53 and the mRNA levels of *CDKN1A* were markedly elevated following sup-tRNA treatment, whereas vector treatment showed minimal efficacy (Fig. 5m, n).

The tumor regression induced by p53 restoration is primarily attributed to p53-mediated apoptosis and growth inhibition[32,33], as evidenced by a reduction in Ki-67 and PCNA-positive proliferating cells, along with an increase in activated caspase-3 and TUNEL-positive apoptotic cells in both xenograft models following sup-tRNA treatment (Fig. 5o). Importantly, safety assessments demonstrated no significant abnormalities in hematological parameters or histopathological evidence of tissue damage in sup-tRNA-treated mice (Extended Data Fig. 6), supporting the favorable therapeutic index of this approach (Fig. 5). Overall, these findings highlight the robust efficacy and excellent safety profile of p53 restoration through sup-tRNA-mediated translational readthrough, warranting further investigation into its broader application in cancer therapy.

Discussion

The distinct biological characteristics of oncogenes and tumor suppressor genes pose fundamentally different challenges for therapeutic intervention. The oncogene addiction in malignant tumors has a compelling therapeutic rationale for the development of targeted therapies[34,35], such as kinase inhibitors[36] and PROTACs[37], which aim to inhibit or degrade hyperactive proteins. In contrast, tumor suppressor genes that often harbor loss-of-function mutations, typically require functional protein restoration, posing a significant pharmacological challenge[4,5]. Furthermore, mutant tumor suppressor proteins

not only lose tumor-suppressive functions, but can also actively antagonize reintroduced wild-type proteins through dominant negative effect, limiting the therapeutic efficacy of gene therapy[11,12,38]. In this work, we showed that sup-tRNA could address these challenges by simultaneously restoring full-length p53 expression while converting dominant-negative truncations into functional variants. Notably, the generation of enhanced suppressor p53 mutants (Fig. 4e, f and Extended Data Fig. 5) through specific amino acid substitution suggests a promising strategy to overcome the therapeutic limit imposed by the transcriptional activity of wild-type p53.

Moreover, we have developed a tailored framework for sup-tRNA in addressing 'undruggable' tumor suppressor mutations[4,5,10,39]. The computational pipeline, which incorporates analysis of readthrough efficiency and structural perturbation, could be adapted to other frequently mutated tumor suppressors such as RB1, PTEN, APC and STK-11 (Fig. 1g, h and Extended Data Fig. 3). Unlike development of traditional small molecules targeting specific mutant proteins, the sup-tRNA strategy is not restricted by protein type and mutation type, as we presented that designed sup-tRNAs could overcome all three types of nonsense mutations across various tumor suppressor genes.

Recent researches have demonstrated that sup-tRNA exhibited extremely low or even no readthrough in normal termination codons, demonstrating the high safety profile of sup-tRNA[25,26]. Consistently, our study showed that sup-tRNA $^{\text{Arg-TCT-3-1}}{}_{\text{TGA}}$ and sup-tRNA$^{\text{Gln-CTG-1-1}}{}_{\text{TAG}}$ induced efficient readthrough in nonsense mutations with no detectable toxicity *in vitro* and *in vivo* (Fig. 4 and Fig. 5). However, in addition to the classical role of tRNAs as mRNA decoders, certain tRNAs could respond to external perturbations and regulate gene expression[40]which either promotes or suppresses tumor progression[41,42]. As engineered from natural tRNAs, certain sup-tRNAs are in theory capable of driving or inhibiting cancer development beyond the readthrough of nonsense

mutations[41,42], suggesting excluding tumor proliferation-related tRNAs in sup-tRNA engineering for cancer therapy.

Overall, this study opens a new avenue for precision oncology that goes beyond the oncogene-centric paradigm. By translating the concept of tumor suppressor restoration into a viable therapeutic strategy, tRNA-based therapy could ultimately redefine treatment strategies for the majority of human cancers driven by suppressor protein inactivation.

Methods

The tumor suppressor gene mutations

The tumor suppressor gene mutation data was downloaded from the COSMIC database (https://cancer.sanger.ac.uk/cosmic) and Intogen database (https://www.intogen.org/). Data of amino acid types of nonsense mutations in tumor suppressor genes collected from the COSMIC database, including *TP53* (COSMIC gene: COSG501), *RB1* (COSMIC gene: COSG16), *PTEN* (COSMIC gene: COSG15) and *APC* (COSMIC gene: COSG257430).

Plasmid construction

Tumor suppressor genes (*TP53, RB1, PTEN, APC*) were constructed in the PCAGGS-FLAG-GUSB-myc-T2A-GFP plasmid. Subsequently, targeted mutations were achieved by introducing primers containing mismatched bases during PCR to obtain plasmids with site-specific nonsense mutations. The tRNAs were constructed in pcDNA3.1(+) vectors and their expression was initiated by the 7SK promoter. tRNA gene sequences were compiled from GtRNA database (http://gtrnadb.ucsc.edu/). PG13-luc (wt p53 binding sites) plasmid (Addgene ID: 16442) were purchased from Addgene. We next changed the luciferase reporter to the mCherry reporter to obtain the plasmid PG13-mCherry. The lactic acid probe pcDNA-FiLa-Cyt and pcDNA-FiLa-C-Cyt

were gifts from Prof Yi Yang of East China University of Science and Technology.

Cell culture and transfection

Human HEK293T cells (ATCC CRL-11268) were cultured in DMEM medium (Procell) as suggested by the repository, supplemented with 10% fetal bovine serum (FBS), 100 U/mL penicillin, 100 mg/mL streptomycin. Human Calu-6 cells (ATCC HTB-56) were cultured MEM medium (Procell) as suggested by the repository, supplemented with 10% fetal bovine serum (FBS), 100 U/mL penicillin, and 100 mg/mL streptomycin. Human Caco-2 cells (ATCC HTB-37) were cultured MEM medium (Procell) as suggested by the repository, supplemented with 20% fetal bovine serum (FBS), 100 U/mL penicillin, and 100 mg/mL streptomycin. All cell lines were tested to be mycoplasma-free and validated by STR profiling. Plasmids were transfected using Lipo3000 and P3000 (Invitrogen). Cell transfections were performed with the supplier's recommendations.

Western blot analysis

The equivalent of 3×10^5 cells was subjected to 10% SDS-PAGE before transferring the proteins to a 0.22um PVDF membrane through eBlot® L1 Fast Wet Transfer System (Genscript, USA). Membranes were incubated overnight at 4 °C in the presence of a 1/200 dilution of anti-p53 antibody (DO1) (Santa Cruz Biotechnology, Dallas, TX, USA; catalog number: sc-126), recognizing human p53. A 1/2000 dilution of anti-P21 antibody (Proteintech, China; catalog number: 10355-1-AP), a 1/100000 dilution of anti-GAPDH antibody (Proteintect, China; catalog number: 1E6D9). After three washes of the membrane in TBS-Tween, the membranes were exposed to a solution of horseradish peroxidase-conjugated secondary antibody for detection of mouse-raised or rabbit-raised antibody (Proteintect, China) at a dilution of 1/2000 (catalog number: SA00001-1, SA00001-2), respectively. Antibodies

were then detected with BeyoECL Moon (P0018FS, Beyotime, China). Photographs were performed with 5200 (Tanon, Shanghai, China). The original unprocessed gel pictures are provided in the source data file. Western blot results were semi-quantitatively analyzed by ImageJ software. Western blot experiments were performed at least third in parallel and representative results were reported. The original western blot images are shown in Supplementary Figs.

qRT-PCR analysis

1.5×10^5 cells per well were seeded in 6-well plates in a final volume of 2 ml. On the following day, cells were transfected with different plasmids of the indicated drugs for 48 h. The RNA extraction was performed using the FastPure Cell/Tissue Total RNA Isolation Kit V2 (Vazyme, China) according to the manufacturer's recommendations. RNA was quantified using a NanoDrop Spectrophotometer (Thermo Scientific, USA). cDNA was synthesized from RNA using Hifair® AdvanceFast One-step RT-gDNA Digestion SuperMix for qPCR (Yeasen, China). Real-time quantitative PCR was performed in the Hieff UNICON® Universal Blue qPCR SYBR Green Master Mix (Yeasen, China) using Roche LightCycler® 480 II (Roche, Switzerland) with the following primers:

GAPDH mRNA (sense: 5′- GGAGCGAGATCCCTCCAAAAT-3′; antisense: 5′-GGCTGTTGTCATACTTCTCATGG-3′).

TP53 mRNA (sense: 5′- CAGCACATGACGGAGGTTGT-3′; antisense: 5′-TCATCCAAATACTCCACACGC -3′).

CDKN1A mRNA (sense: 5′- TGTCCGTCAGAACCCATGC -3′; antisense: 5′-AAAGTCGAAGTTCCATCGCTC -3′).

BBC3 mRNA (sense: 5′- GCCAGATTTGTGAGACAAGAGG -3′; antisense: 5′-CAGGCACCTAATTGGGCTC -3′).

GADD45A mRNA (sense: 5′- GAGAGCAGAAGACCGAAAGGA -3′; antisense: 5′- CACAACACCACGTTATCGGG -3′).

BAX mRNA (sense: 5′- CCCGAGAGGTCTTTTTCCGAG -3′; antisense: 5′-CCAGCCCATGATGGTTCTGAT -3′).

ZMAT3 mRNA (sense: 5′- AGAAGCCTTTTGGGCAGGAG -3′; antisense: 5′-TGCTGCATAGTAATTTCGGAGTT -3′).

FAS mRNA (sense: 5′- TCTGGTTCTTACGTCTGTTGC -3′; antisense: 5′-CTGTGCAGTCCCTAGCTTTCC -3′).

PMAIP1 mRNA (sense: 5′- ACCAAGCCGGATTTGCGATT -3′; antisense: 5′-ACTTGCACTTGTTCCTCGTGG -3′).

The relative expression fold was calculated by the $2^{-\Delta\Delta Ct}$ equation.

PCR array

Cell transfected, total RNA extracted and cDNA synthesized as described above. cDNA mixed with qPCR SYBR, added into the p53 PCR Array 96- well plate (WcGENE Biotech, WC-MRNA0117-H) to detect the expression of a set of p53-related genes.

Colony formation assay

After 8 hours of transfection, we digested and resuspended the cells. We planted cancer cells into the six-well plate at a density of 1000 cells/well and then cultured them in a complete culture medium at 37°C for 7-10 days. After being gently washed in PBS twice, the cells were fixed with 4% paraformaldehyde fix solution for 30 min. Crystal Violet Staining Solution (Beyotime, China; catalog number: C0121) was applied for staining the fixed cells for 30 min. IncuCyte SX5 imaging system (Sartorius AG, Goettingen, Germany) was used to count the number of colonies, total colonies area, and individual clone area.

Cell growth curve analysis

Cell transfected, digested, and resuspended as described above. For the cell counting, cells were inoculated into a 24-well plate with an appropriate number of cells, digested at 24h, 48h, 72h, and 96h after inoculation, and then counted

by cell counter (Countstar BioTech, China). For the CCK-8 assays, cells were seeded into a 96-well plate at 2000 cells per well. According to the protocol of CCK-8 solution (Beyotime, China; catalog number: C0040), 10 μl of CCK-8 solution diluted in 100 μl of complete culture medium replaced the original medium of each group at indicated points. After the cells were incubated in the dark at 37 °C for an additional 1 h, we detected viable cells by using absorbance at a 450nm wavelength through Microplate Reader AMR-100(Allsheng, China).

The landscape of gene mutation

The STAR-counts data and mutation maf data of tumors were downloaded from the TCGA database (https://portal.gdc.cancer.gov). The data in TPM format was subsequently extracted from the STAR-counts data and normalized using log2(TPM+1). The samples that had RNAseq data, maf mutation data, and clinical information were then retained. The maftools package in R software was utilized to download and visualize the somatic mutations of patients. Statistical analysis was conducted using R software, version v4.0.3.

Molecular dynamics simulation

The molecular dynamics simulations of all studied protein/DNA complexes were performed with the AMBER 22 molecular simulation package. The crystal structure of tumor-suppressor protein p53/DNA complex (PDB code: 2AC0) was used for the calculation. The starting structures of all molecular systems were solvated in TIP3P water using an octahedral box, which extended 8 Å away from any solute atom. To neutralize the negative charges of simulated molecules, Na+ counter-ions were placed next to each negative group. MD simulations were carried out by using the PMEMD module of AMBER 22. The calculation began with 500 steps of steepest descent followed by 500 steps of conjugate gradient minimization with a large constraint of 500 kcal mol-1 Å-2

on the atoms of the protein and DNA. Then 1000 steps of steepest descent followed by 4000 steps of conjugate gradient minimization with no restraint on the complex atoms were performed. Subsequently, after 200 ps of MD, during which the temperature was slowly raised from 0 to 300 K with weak (5 kcal mol-1Å-2) restraint on the protein/DNA, the final unrestrained production simulations of 200.0 ns were carried out at constant pressure (1 atm) and temperature (300 K). In the entire simulation, SHAKE was applied to all hydrogen atoms. Periodic boundary conditions with minimum image conventions were applied to calculate the non-bonded interactions. A cutoff of 10 Å was used for the Lennard–Jones interactions. The final respective conformations of all the protein/DNA complexes used for discussion were produced from the last 50.0 ns of MD.

Whole-transcriptome analysis

Total RNA was extracted from tumor xenograft of different mice (three replicates for each group) using TRIzol reagent. RNA libraries were constructed using the VAHTS Universal V6 RNA-seq Library Prep Kit for Illumina (Vazyme, NR604-02) according to the manufacturer's instructions. The concentration of the extracted RNA was detected using the Nanodrop2000 (Thermo Fisher, Nanodrop2000), and its integrity was tested using the Agilent 2100 (Vazyme, G2939BA). The quality and quantity of the constructed libraries were assessed using the BioAnalyzer 2100 system (Agilent Technologies).

Subsequently, the libraries were sequenced on an Illumina NovaSeq X Plus platform with 150-bp paired-end reads. The sequencing data were quality-controlled using the Q30 metric. After adapter trimming at the 3' end and removing low-quality reads with the fastp(https://github.com/OpenGene/fastp, fastp-V0.20.1), high-quality clean reads were aligned to the reference genome using the HISAT2(https://daehwankimlab.github.io/hisat2/, hisat2-2.0.4).

Guided by the gffcompare, the ballgown software package was used to obtain

gene-level FPKM (Fragments Per Kilobase of transcript per Million mapped reads) values as the expression profiles of mRNA. The total number of expressed genes and the log2FPKM values of mRNA in different tumor xenograft groups were plotted and compared. Significant differences between samples were analyzed using DEseq2, and genes with a multiplicity of difference FoldChange>2 times and P-value<0.01 were defined as differential genes and subsequently analyzed.

Xenograft tumor model

Animal experiments were proven by the Institutional Animal Care and Use Committee of Peking University Health Science Center (Animal Protocol ID: DLASBD0468). Female BALB/c nude mice aged 6-8 weeks were housed in an SPF facility in a 12-h light-dark cycle and allowed free access to water and food. To develop the tumor, calu-6 cells (5×10^6 cells/mouse; 1:1 suspended in BD Matrigel™) and caco-2 cells (1×10^7 cells/mouse; 1:1 suspended in BD Matrigel™) were injected into the substance of each mouse (day 0). Tumor volumes and mice weight were calculated every 2 days, tumor volumes using the following standard formula: volume = 0.5 × length × width^2. Sup-tRNAs were delivered to the tumor through dendrimer nanoparticles. Mice were sacrificed after treatment. Tumors were dissected, weighed, and cut in thirds: one-third was frozen in liquid nitrogen for protein analysis, one-third was kept in the RNAlater (Beyotime, China; catalog number: R0118) for RT-qPCR analysis and one-third was fixed in 4% paraformaldehyde (PFA) for histological analysis and immunostaining.

Immunofluorescence staining

Collected tumors were fixed in 4% PFA at room temperature and prepared as 10-μm tumor sections. For p53 and CDKN1A, antigens were repaired by Tris-EDTA antigen repair solution G1206 (Servicebio, Wuhan, China). For ki67, PCNA and caspase-3, the antigen was repaired by Citric Acid Antigen Repair

Solution G1202 (Servicebio, Wuhan, China). For quenching of endogenous peroxidase, the sections were incubated in 3% hydrogen peroxide solution for 25 min at room temperature, protected from light, and the slides were placed in PBS (pH 7.4) and washed three times for 5 min each time by shaking on a shaker. 3% BSA was then added to cover the tissue evenly and closed for 30 min at room temperature. The blocking solution was removed and sections were incubated with diluted primary antibody at 4°C overnight in a wet box, 1/50 dilution of anti-p53 antibody (DO1) (Santa Cruz Biotechnology, Dallas, TX, USA; catalog number: sc-126), recognizing human p53. 1/200 dilution of anti-P21 antibody (Proteintect, China; catalog number: 10355-1-AP). 1/200 dilution of anti-ki67 antibody (Servicebio, China; catalog number: GB121141). 1/200 dilution of anti-PCNA antibody (Servicebio, China; catalog number: GB12010). A 1/200 dilution of anti-cas3 antibody (Servicebio, China; catalog number: GB11532). After washed in PBS on a decolorizing shaker with shaking three times, 5 min each time, sections were shaken dry and the tissue was covered with a drop of secondary antibody (HRP-labelled) of the corresponding species to the primary antibody and incubated for 50 min at room temperature. The slides were subsequently shaken dry after washing and freshly prepared DAB color development solution G1212 (Servicebio, Wuhan, China) was added dropwise, while the time of color development was controlled under the microscope. The sections were counterstained in hematoxylin followed by dehydration with graded ethanol, n-butanol, and xylene, then the sections were taken out of xylene to dry and seal. The slides were photographed under pathology slide scanner ws-10 (Wisleap, China). NDPView2 software (Hamamatsu, Japan) was used to analyze and record these images.

Histological analysis

Blood samples from mice were collected from the orbital vein, and stored in the tube with K2-ethylenediaminetetraacetic acid (EDTA) at 4°C. The

hematological parameters were analyzed using a BC-2800Vet® Auto Hematology Analyzer (Shenzhen Mindray Bio-Medical Electronics Co., Ltd, Hamburg, Germany). The heart, liver, spleen, lung, and kidney tissues from different groups of mice were isolated and fixed in 4% PFA. They were then sequentially dehydrated in 70%, 95%, and 100% ethanol, followed by defatting with xylene for 2 hours before being embedded in paraffin. The 10-μm-thick sections were obtained and subjected to H&E staining. The slices were examined using a pathology slide scanner (WS-10, Wisleap, China). Image analysis and recording were performed using NDPView2 software (Hamamatsu, Japan).

Statistical analysis

Data were analyzed using the GraphPad Prism v5 statistical software package (GraphPad Software, La Jolla, CA). Data were expressed as means ± SD. The one-way analysis of variance (ANOVA) with Newman-Keuls multiple comparisons test with statistical significance set at $P < 0.001$ was performed. Appropriate statistical tests have been mentioned in figure legends.

Acknowledgements

We are grateful to Y. Zhao and S. Shu for comments and feedbacks on this article. This work was financially supported by the National Key R&D Program of China, Frontier Biotechnology, (Grant No. 2023YFC3403300) and the National Natural Science Foundation of China (Grant No. U23A20106).

Author contributions

Q.X. and B.K. conceived the idea and designed the experiments. B.K. and Z.Z. performed the experiments and offered the original data. B.K., Z.D., Y.Y., and Y.S. provided materials for plasmid cloning. B.K., Z.M., Y.L. and J.L. conducted the animal experiments. B.K., Z.Z. and Q.X. organized the results and wrote

the manuscript. All authors participated in data discussion and interpretation. Q.X. supervised the study.

Competing interests

Q.X. and B.K. are inventors on patents regarding the suppressor tRNA for tumor suppressor protein recovery. Q.X. is the founder of QiXia Decode Biotechnology Co., Ltd. and holds equity in this company. The other authors declare no competing interests.

Additional information

Correspondence and requests for materials should be addressed to Qing Xia.

Reference

1 Stratton, M. R., Campbell, P. J. & Futreal, P. A. The cancer genome. *Nature* **458**, 719-724, doi:10.1038/nature07943 (2009).

2 Martinez-Jimenez, F. *et al.* A compendium of mutational cancer driver genes. *Nat Rev Cancer* **20**, 555-572, doi:10.1038/s41568-020-0290-x (2020).

3 Stratton, M. R. Exploring the genomes of cancer cells: progress and promise. *Science* **331**, 1553-1558, doi:10.1126/science.1204040 (2011).

4 Prasad, V. Perspective: The precision-oncology illusion. *Nature* **537**, S63, doi:10.1038/537S63a (2016).

5 Tannock, I. F. & Hickman, J. A. Limits to Personalized Cancer Medicine. *N Engl J Med* **375**, 1289-1294, doi:10.1056/NEJMsb1607705 (2016).

6 Mendiratta, G. *et al.* Cancer gene mutation frequencies for the U.S. population. *Nat Commun* **12**, 5961, doi:10.1038/s41467-021-26213-y (2021).

7 Mendiratta, G., Jones, M. K. & Stites, E. C. How often is each gene mutated within the cancer patient population? *Mol Cell Oncol* **9**, 2065176, doi:10.1080/23723556.2022.2065176 (2022).

8 Tuval, A., Strandgren, C., Heldin, A., Palomar-Siles, M. & Wiman, K. G. Pharmacological reactivation of p53 in the era of precision anticancer medicine. *Nat Rev Clin Oncol* **21**, 106-120, doi:10.1038/s41571-023-00842-2 (2024).

9 Brogna, S. & Wen, J. Nonsense-mediated mRNA decay (NMD) mechanisms. *Nat Struct Mol Biol* **16**, 107-113, doi:10.1038/nsmb.1550 (2009).

10 Dang, C. V., Reddy, E. P., Shokat, K. M. & Soucek, L. Drugging the 'undruggable' cancer targets. *Nat Rev Cancer* **17**, 502-508, doi:10.1038/nrc.2017.36 (2017).

11 Peuget, S., Zhou, X. & Selivanova, G. Translating p53-based therapies for cancer into the clinic. *Nat Rev Cancer* **24**, 192-215, doi:10.1038/s41568-023-00658-3 (2024).

12 Song, H., Xiao, S., Wu, J. & Lu, M. Drugging p53: Barriers, Criteria, and Prospects. *Cancer Discov* **14**, 2055-2060, doi:10.1158/2159-8290.CD-24-0837 (2024).

13 Levine, A. J. & Oren, M. The first 30 years of p53: growing ever more complex. *Nat Rev Cancer* **9**, 749-758, doi:10.1038/nrc2723 (2009).

14 Glimmers of Hope for Targeting p53. *Cancer Discov* **12**, OF5, doi:10.1158/2159-8290.CD-ND2022-0009 (2022).

15 Chen, S. *et al.* Arsenic Trioxide Rescues Structural p53 Mutations through a Cryptic Allosteric Site. *Cancer Cell* **39**, 225-239 e228, doi:10.1016/j.ccell.2020.11.013 (2021).

16 Song, H. *et al.* Diverse rescue potencies of p53 mutations to ATO are predetermined by intrinsic mutational properties. *Sci Transl Med* **15**, eabn9155,

752 doi:10.1126/scitranslmed.abn9155 (2023).

753 17 Li, J. *et al.* Pharmacological rescue of mutant p53 triggers spontaneous tumor
754 regression via immune responses. *Cell Rep Med*, 101976,
755 doi:10.1016/j.xcrm.2025.101976 (2025).

756 18 Oren, M. & Prives, C. p53: A tale of complexity and context. *Cell* **187**, 1569-1573,
757 doi:10.1016/j.cell.2024.02.043 (2024).

758 19 Keeling, K. M. & Bedwell, D. M. Clinically relevant aminoglycosides can suppress
759 disease-associated premature stop mutations in the IDUA and P53 cDNAs in a
760 mammalian translation system. *J Mol Med (Berl)* **80**, 367-376,
761 doi:10.1007/s00109-001-0317-z (2002).

762 20 Floquet, C., Deforges, J., Rousset, J. P. & Bidou, L. Rescue of non-sense mutated
763 p53 tumor suppressor gene by aminoglycosides. *Nucleic Acids Res* **39**, 3350-3362,
764 doi:10.1093/nar/gkq1277 (2011).

765 21 Trzaska, C. *et al.* 2,6-Diaminopurine as a highly potent corrector of UGA nonsense
766 mutations. *Nat Commun* **11**, 1509, doi:10.1038/s41467-020-15140-z (2020).

767 22 Palomar-Siles, M. *et al.* Translational readthrough of nonsense mutant TP53 by
768 mRNA incorporation of 5-Fluorouridine. *Cell Death Dis* **13**, 997,
769 doi:10.1038/s41419-022-05431-2 (2022).

770 23 Strandgren, C. & Wiman, K. G. Therapeutic targeting of TP53 nonsense mutations in
771 cancer. *Ups J Med Sci* **129**, doi:10.48101/ujms.v129.10719 (2024).

772 24 Lueck, J. D. *et al.* Engineered transfer RNAs for suppression of premature termination
773 codons. *Nat Commun* **10**, 822, doi:10.1038/s41467-019-08329-4 (2019).

25 Wang, J. *et al.* AAV-delivered suppressor tRNA overcomes a nonsense mutation in mice. *Nature* **604**, 343-348, doi:10.1038/s41586-022-04533-3 (2022).

26 Albers, S. *et al.* Engineered tRNAs suppress nonsense mutations in cells and in vivo. *Nature* **618**, 842-848, doi:10.1038/s41586-023-06133-1 (2023).

27 Cheng, J. *et al.* Accurate proteome-wide missense variant effect prediction with AlphaMissense. *Science* **381**, eadg7492, doi:10.1126/science.adg7492 (2023).

28 Bendl, J. *et al.* PredictSNP: robust and accurate consensus classifier for prediction of disease-related mutations. *PLoS Comput Biol* **10**, e1003440, doi:10.1371/journal.pcbi.1003440 (2014).

29 Kakudo, Y., Shibata, H., Otsuka, K., Kato, S. & Ishioka, C. Lack of correlation between p53-dependent transcriptional activity and the ability to induce apoptosis among 179 mutant p53s. *Cancer Res* **65**, 2108-2114, doi:10.1158/0008-5472.CAN-04-2935 (2005).

30 Funk, J. S. *et al.* Deep CRISPR mutagenesis characterizes the functional diversity of TP53 mutations. *Nat Genet* **57**, 140-153, doi:10.1038/s41588-024-02039-4 (2025).

31 Boettcher, S. *et al.* A dominant-negative effect drives selection of TP53 missense mutations in myeloid malignancies. *Science* **365**, 599-604, doi:10.1126/science.aax3649 (2019).

32 Ventura, A. *et al.* Restoration of p53 function leads to tumour regression in vivo. *Nature* **445**, 661-665, doi:10.1038/nature05541 (2007).

33 Xue, W. *et al.* Senescence and tumour clearance is triggered by p53 restoration in murine liver carcinomas. *Nature* **445**, 656-660, doi:10.1038/nature05529 (2007).

34 Weinstein, I. B. & Joe, A. K. Mechanisms of disease: Oncogene addiction--a rationale for molecular targeting in cancer therapy. *Nat Clin Pract Oncol* **3**, 448-457, doi:10.1038/ncponc0558 (2006).

35 Weinstein, I. B. & Joe, A. Oncogene addiction. *Cancer Res* **68**, 3077-3080; discussion 3080, doi:10.1158/0008-5472.CAN-07-3293 (2008).

36 Attwood, M. M., Fabbro, D., Sokolov, A. V., Knapp, S. & Schioth, H. B. Trends in kinase drug discovery: targets, indications and inhibitor design. *Nat Rev Drug Discov* **20**, 839-861, doi:10.1038/s41573-021-00252-y (2021).

37 Tsai, J. M., Nowak, R. P., Ebert, B. L. & Fischer, E. S. Targeted protein degradation: from mechanisms to clinic. *Nat Rev Mol Cell Biol* **25**, 740-757, doi:10.1038/s41580-024-00729-9 (2024).

38 Liu, Y., Su, Z., Tavana, O. & Gu, W. Understanding the complexity of p53 in a new era of tumor suppression. *Cancer Cell* **42**, 946-967, doi:10.1016/j.ccell.2024.04.009 (2024).

39 Sabapathy, K. & Lane, D. P. Therapeutic targeting of p53: all mutants are equal, but some mutants are more equal than others. *Nat Rev Clin Oncol* **15**, 13-30, doi:10.1038/nrclinonc.2017.151 (2018).

40 Torrent, M., Chalancon, G., de Groot, N. S., Wuster, A. & Madan Babu, M. Cells alter their tRNA abundance to selectively regulate protein synthesis during stress conditions. *Sci Signal* **11**, doi:10.1126/scisignal.aat6409 (2018).

41 Pinzaru, A. M. & Tavazoie, S. F. Transfer RNAs as dynamic and critical regulators of cancer progression. *Nat Rev Cancer* **23**, 746-761, doi:10.1038/s41568-023-00611-4

(2023).

42 Goodarzi, H. *et al.* Modulated Expression of Specific tRNAs Drives Gene Expression and Cancer Progression. *Cell* **165**, 1416-1427, doi:10.1016/j.cell.2016.05.046 (2016).